

See discussions, stats, and author profiles for this publication at: <https://www.researchgate.net/publication/10982687>

Structures and Cytotoxic Properties of Sponge-Derived Bisannulated Acridines

ARTICLE in THE JOURNAL OF ORGANIC CHEMISTRY · JANUARY 2003

Impact Factor: 4.72 · DOI: 10.1021/jo026459o · Source: PubMed

CITATIONS

45

READS

25

10 AUTHORS, INCLUDING:



Karen Tenney

University of California, Santa Cruz

56 PUBLICATIONS 1,301 CITATIONS

SEE PROFILE



Fred Valeriote

Henry Ford Hospital

241 PUBLICATIONS 5,385 CITATIONS

SEE PROFILE



Phil Crews

University of California, Santa Cruz

179 PUBLICATIONS 6,187 CITATIONS

SEE PROFILE

Structures and Cytotoxic Properties of Sponge-Derived Bisannulated Acridines

Zia Thale,[†] Tyler Johnson,[†] Karen Tenney,[†] Philip J. Wenzel,[†] Emil Lobkovsky,[‡] Jon Clardy,[‡] Joe Media,[§] Halina Pietraszkiewicz,[§] Frederick A. Valeriote,[§] and Phillip Crews^{*,†}

Department of Chemistry and Biochemistry and Institute for Marine Sciences, University of California, Santa Cruz, California 95064, Department of Chemistry and Chemical Biology, Cornell University, Ithaca, New York 41853-1301, and Josephine Ford Cancer Center, Henry Ford Health Systems, Detroit, Michigan 48202

phil@chemistry.ucsc.edu

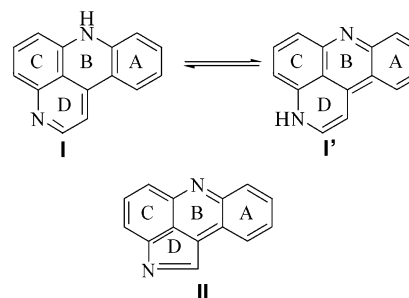
Received September 18, 2002

A reinvestigation of sponge natural products from additional Indo-Pacific collections of *Xestospongia* cf. *carbonaria* and *X. cf. exigua* has provided further insights on the structures, biological activities, and biosynthetic origin of bisannulated acridines. These alkaloids include one known pyridoacridine, neoamphimedine (**2**), and three new analogues, 5-methoxyneoamphimedine (**4**), neoamphimedine Y (**5**), and neoamphimedine Z (**6**). A completely new acridine, alpinkidine (**7**), was also isolated. A disk diffusion soft agar assay, using a panel of five cancer cell lines (solid tumors and leukemias) and two normal cells, was used to evaluate the differential cytotoxicity (solid tumor selectivity) of the sponge semipure extracts and selected compounds including amphimedine (**1**), **2**, **4**, and **7**. While all four compounds were solid tumor selective, **1** and **2** were the most potent and **4** was the most selective. The rationale used to characterize the new structures is outlined along with the related biosynthetic pathways envisioned to generate **2** and **7**.

Introduction

Marine-derived zoonchroic alkaloids possessing a bisannulated acridine core possess striking structures and broad biological activity. Subsets of this class, commonly referred to as pyridoacridines and pyrroloacridines, have additional appeal because of their distribution in both marine sponges and tunicates.¹ A pyridoacridine has a six-membered D-ring fused to an A/B/C acridine core shown in **I** and **I'**, whereas a pyrroloacridine has a contracted D-ring as shown in **II**.² All of the more than 55 pyridoacridines and pyrroloacridines reported to date are from marine sources. Significantly, members of these two families are active in assays for antihelmintic,² antitumor,^{2,3} antifungal,⁴ and DNA binding.^{5–7} There have been several prior investigations on two related sponges, *Xestospongia carbonaria* and *Xestospongia*

CHART 1



exigua, which have been an occasional source of bisannulated acridines. Our attention was drawn to these two species because their extracts were potently active in a primary screen. The screen consists of a disk diffusion soft agar assay, using a panel of five cancer cell lines (solid tumors and leukemias) and two normal cells to evaluate differential cytotoxicity.⁸ The power of this approach has been clearly demonstrated in the isolation and development of the cryptophycins that were recently advanced to clinical trials.⁹ This assay has effectively guided some of our research on Indo-Pacific sponges and we believe it is has been further validated by the positive results obtained in this investigation. The deep color of the extracts along with taxonomic considerations suggested that one or more substituted acridines might be present, possibly explaining the bioactivity of the crude extracts. Therefore, we launched an assay-guided isola-

* To whom correspondence should be addressed. Phone: 831-459-2603. E-mail: phil@chemistry.ucsc.edu.

[†] University of California.

[‡] Cornell University.

[§] Henry Ford Health Systems.

(1) Molinski, T. F. *Chem. Rev.* **1993**, *93*, 1825–1838.

(2) Inman, W. D.; O'Neill-Johnson, M.; Crews, P. *J. Am. Chem. Soc.* **1990**, *112*, 1–4.

(3) Gimenez-Arnau, E.; Missailidis, S.; Stevens, M. F. G. *Anti-Cancer Drug Res.* **1998**, *13*, 431–451.

(4) McCarthy, P. J.; Pitts, T. P.; Gunawardana, G. P.; Kelly-Borges, M.; Pomponi, S. A. *J. Nat. Prod.* **1992**, *55*, 1664–1668.

(5) Shochet, N. R.; Rudi, A.; Kashman, Y.; Hod, Y.; El-Maghrabi, M. R.; Spector, I. *J. Cell Physiol.* **1993**, *157*, 481–492.

(6) Tasdemir, D.; Marshall, K. M.; Mangalindan, G. C.; Concepción, G. P.; Barrows, L. R.; Harper, M. K.; Ireland, C. M. *J. Org. Chem.* **2001**, *66*, 3246–3248.

(7) McDonald, L. A.; Eldredge, G. S.; Barrows, L. R.; Ireland, C. M. *J. Med. Chem.* **1994**, *37*, 3819–3827.

(8) Sperry, S.; Valeriote, F. A.; Corbett, T. H.; Crews, P. *J. Nat. Prod.* **1998**, *61*, 241–247.

TABLE 1. Zone Unit Differentials in the Disk Diffusion Soft Agar Colony Formation Assay^a

entry no.	solvent partition fractions ^b	murine tumor selectivity			human tumor selectivity	
		concn, ug/disk	Z _{C38} –Z _{L1210}	Z _{C38} –Z _{CFU–GM}	Z _{H116\H125} –Z _{CEM}	Z _{H116\H125} –Z _{CFU–GM}
	<i>X. cf. exigua</i> (coll. no. 91608)					
1	FD	150	200	250	350\350	150\200
2	FM	300	400	350	100\200	
3	WB	280	400	400	–50\50	
4	DMM	320	300	450	100\200	
5	FH	260	200	150	ND*	
6	DMH	200	150	ND	–50/0	
	<i>X. cf. carbonaria</i> (coll. no. 94634)					
7	FD	25	0	150	150\350	–200\0
8	FM		50	150	550\400	
9	WB	100	50	150	–50\200	
10	DMM	100	350	250	300\400	–\300
11	FH	100	–50	ND	ND	
12	DMH	100	450	250	100\100	
	compounds					
13	amphimedine (1)	3.75	300	350	ND	
14	neoamphimedine (2)	2.4	200	250	250\350	250\350
15	5-methoxyneoamphimedine (4)	25	>700	>800	–250\–150	
16	alpinidine (7)	120	300	300	ND	

^a Measured in zone units: 200 zone units = 6 mm. Murine cell lines: L1210 (lymphocytic leukemia), C38 (colon adenocarcinoma), CFU-GM (colony-forming unit-granulocyte macrophage; normal hematopoietic). Human cell lines: H116 (colon), H125 (lung), CEM (leukemia), CFU-GM (colony-forming unit-granulocyte macrophage; normal hematopoietic). ^b Solvent partition fraction codes are outlined in the Experimental Section. *ND = not determined as the zone units for H116, H125, or C38 were <250.

tion first to characterize the constituents and then explore their selective cytotoxicities. Reported below are the structures and properties of five different alkaloids including a set of pyridoacridines headed by the known neoamphimedine (2), accompanied by three new neoamphimedine analogues, 5-methoxyneoamphimedine (4), neoamphimedine Y (5), and neoamphimedine Z (6), along with one completely new pyrroloacridine, alpkindine (7).

Results and Discussion

The extracts of *Xestospongia cf. exigua* (coll. no. 91608) and *Xestospongia cf. carbonaria* (coll. no. 94634) displayed *in vitro* selectivity against a panel of human and murine tumor cells. The supporting data are shown in Table 1 (also see Table S1) and solid tumor selectivity is defined as a differential in kill zone units equal to or greater than 250 between any solid tumor cell line and either a normal or a leukemia cell. Both semipure extract fractions of collection numbers *X. cf. exigua* (Table 1, entry no. 1) and *X. cf. carbonaria* (Table 1, entry no. 11) demonstrated differential cytotoxicity of 250 units or greater for solid tumor vs normal cells. This selectivity for solid tumor cells provided the basis for the bioassay guided isolation.

As the isolation work proceeded, it seemed likely, as noted above, that bisannulated acridines were present in the crude extracts. Therefore, especially relevant were the properties of the 17-bisannulated acridines previously reported from sponges and divisible into five families

based on the tetracyclic core of **I****I'** or **II**.¹⁰ One additional consideration was recent literature indicating that the unambiguous characterization of bisannulated acridines could be problematic despite the power of contemporary approaches to organic structure determination.¹¹

Some of the challenges to be dealt with were highlighted in the structure elucidation of amphimedine (1), the first reported pyridoacridine.¹¹ A major difficulty came from the lack of information content in the ¹H NMR spectrum owing to the high ratio of C + N + O to nonaliphatic H's (in this case equal to 3.0). Subsequent investigations of bisannulated acridines were often beleaguered by similar difficulties.¹² For example, there was a protracted time period associated with the full characterization of neoamphimedine (2), a regioisomer of amphimedine (1), consistently isolated from *Xestospongia carbonaria*. Its structure first appeared without supporting details in Molinski's 1993 review paper,¹ then it was included in a 1996 UCSC Ph.D. dissertation,¹³ and it was

(9) (a) Trimurtulu, G.; Ohtani, I.; Patterson, G. M. L.; Moore, R. E.; Corbett, T. H.; Valeriote, F. A.; Demchik, L. *J. Am. Chem. Soc.* **1994**, *116*, 4729–4737. (b) Corbett, T. H.; Valeriote, F. A.; Demchik, L.; Polin, L.; Panchapor, C.; Pugh, S.; White, K.; Knight, J.; Jones, J.; Jones, L.; LoRusso, P.; Foster, B.; Wiegand, R. A.; Lisow, L.; Golakoti, T.; Heltzel, C. E.; Ogino, J.; Patterson, G. M.; Moore, R. E. *J. Exp. Ther. Oncol.* **1996**, *1*, 95–108. (c) Menon, K.; Alvarez, E.; Forler, P.; Phares, V.; Amsrud, T.; Shih, C.; Al-Awar, R.; Teicher, B. A. *Cancer Chem. Pharm.* **2000**, *46*, 142–149.

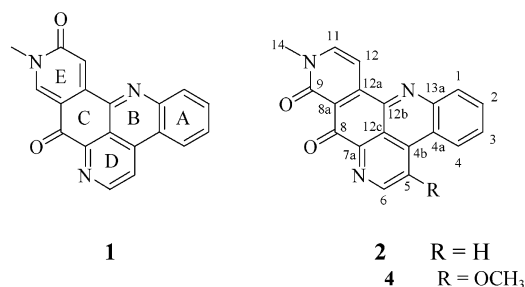
(10) These are summarized in Table S2 as ring type **I-A** (see **1** and **2**), **I-B** (e.g., meridine), **I-C** (e.g., cystodamine), **I-D** (e.g., dercitamide), and **II-E** (see **3**) with the examples of the former greatly outnumbering the latter. (a) Ford, P. W.; Davidson, B. S. *J. Nat. Prod.* **1997**, *60*, 1051–1053. (b) Smith, C. J.; Venables, D. A.; Hopmann, C.; Salomon, C. E.; Jompa, J.; Tahir, A.; Faulkner, D. J.; Ireland, C. M. *J. Nat. Prod.* **1997**, *60*, 1048–1050. (c) West, R. R.; Mayne, C. L.; Ireland, C. M.; Brinen, L. S.; Clardy, J. *Tetrahedron Lett.* **1990**, *31*, 3271–3274.

(11) Schmitz, F. J.; Agarwal, S. K.; Gunasekera, S. P.; Schmidt, P. G.; Shoolery, J. N. *J. Am. Chem. Soc.* **1983**, *105*, 4835–4836.

(12) (a) Koren-Goldshlager, G.; Akinin, M.; Gaydou, E. M.; Kashman, Y. *J. Org. Chem.* **1998**, *63*, 4601–4603. (b) Searle, P. A.; Molinski, T. F. *J. Org. Chem.* **1994**, *59*, 6600–6605. (c) Plubrukarn, A.; Davidson, B. S. *J. Org. Chem.* **1998**, *63*, 1657–1659. (d) Copp, B. R.; Jompa, J.; Tahir, A.; Ireland, C. M. *J. Org. Chem.* **1998**, *63*, 8024–8026. (e) Eder, C.; Schupp, P.; Proksch, P.; Wray, V.; Steube, K.; Müller, C. E.; Frobenius, W.; Herderich, M.; van Soest, R. W. M. *J. Nat. Prod.* **1998**, *61*, 301–305. (f) Koren-Goldshlager, G.; Akinin, M.; Kashman, Y. *J. Nat. Prod.* **2000**, *63*, 830–831. (g) Bontemps, N.; Bonnard, I.; Banaigs, B.; Combaut, G.; Francisco, C. *Tetrahedron Lett.* **1994**, *35*, 7023–7026.

(13) Farias, J. J. Ph.D. Dissertation. Novel Tryptamine Heteroaromatics Isolated from Marine Sponges: Potential Leads for Anticancer Compounds. University of California: Santa Cruz, CA, 1996; pp 101–123.

CHART 2



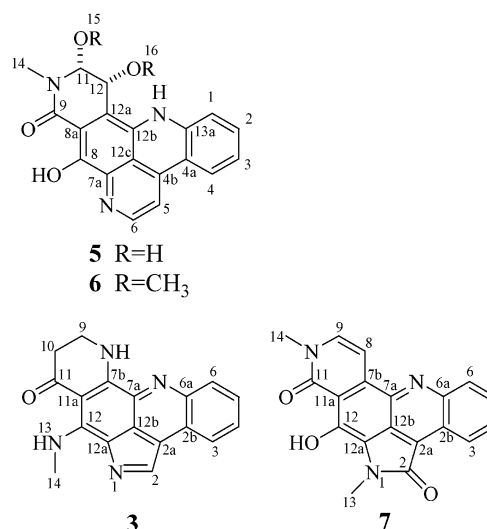
finally formally reported in 1999 as a novel topoisomerase II inhibitor.¹⁴

Though an *Amphimedon* sp. was the initial source of **1**,¹¹ sponges of the genus *Xestospongia* sp. also contained amphimedine (**1**)^{6,9b,14} and 9-deoxyamphimedine.^{6,14} By contrast some collections of *Xestospongia* sometimes afforded mero-sesquiterpenes such as the halenaquinones,¹⁵ halenaquinols,¹⁶ xestoquinones,^{15a,17} and xestoquinolides.^{17b} Thus, based on chemotaxonomy, the potential scope of the chemistry to be encountered initially seemed broad. Parallel examination of the *X. cf. exigua* and *X. cf. carbonaria* extracts by analytical HPLC with diode array UV detection revealed a similar content of bisannulated acridines while no sesquiterpenes were observed. In fact, there was one major metabolite common to both sponge extracts, and it was identified as neoamphimedine (**2**).

The extract of *Xestospongia cf. exigua* (coll. no. 91608) was examined first as it appeared by NMR and HPLC to be the least complex. Each of the six Kupchan-type solvent partition fractions⁸ obtained was evaluated in the disk diffusion soft agar assay. The most potent fraction (Table 1, entry no. 1) was chosen for further HPLC purification, which afforded **2** plus 5-methoxyneoamphimedine (**4**). Interestingly, the murine tumor selectivity data (Table 1 entry 1 vs entries 15 and 16) showed both compounds were more potent and selective than their semipure extract fraction source, indicating that the bioassay approach was effective.

A more complex mixture was presented by the extract of *Xestospongia cf. carbonaria* (coll. no. 94634) that was also subdivided into six Kupchan-type solvent partition fractions.⁸ One of these (Table 1, entry no. 11) possessed murine tumor selectivity as well as human solid tumor selectivity and it was selected for further investigation. The purification began with chromatography over a

CHART 3



Diaion HP20 column followed by gradient reverse-phase HPLC affording neoamphimedine (**2**), 5-methoxyneoamphimedine (**4**), neoamphimedine Y (**5**), neoamphimedine Z (**6**), and alpinkidine (**7**).

The dereplication and structural characterizations of the compounds isolated were conducted as follows. First, the individual samples of neoamphimedine (**2**) and 5-methoxyneoamphimedine (**4**), obtained as yellow-brown solids from both *X. cf. carbonaria* and *X. cf. exigua*, were each combined for further analysis. The HRESIMS and ¹H and ¹³C NMR data (Table 2) of **2** were consistent with the published properties.¹⁴ Second, the characterization of **4** began with side-by-side interpretation of its ¹H NMR, ¹³C NMR, and MS data, with the properties of **2** also serving as an obvious benchmark. Thus, the molecular formula of **4** was established as C₂₀H₁₄N₃O₃, from HRESIMS data (344.1044 *m/z*), and it differed from that of **2** by an additional OCH₂. Its ¹³C NMR spectrum (Table 2) revealed 16 vinyl carbon atoms, two carbonyls (δ 177.9, 158.5), a NCH₃ (δ 38.0), and a OCH₃ (δ 58.0). Also consistent with these features were resonances in the ¹H NMR spectrum for two heteroatom attached CH₃ groups along with seven aromatic protons, as compared to the single NCH₃ group and six aromatic protons present in **2**. The logical assumption of replacement of an aromatic proton in **2** by an OCH₃ group appeared correct but establishing its exact location needed additional analysis. The OCH₃ had to be attached to ring D as the shifts and spin systems of H11 and H12 as well as those of H1–4 were still intact. Model compound ¹³C NMR shift calculations carried out with the aid of the ACD¹⁸ software package provided data for 5-methoxyneoamphimedine (C5/C6: δ 148s/131d) and 6-methoxyneoamphimedine (C5/C6: δ 170s/100d) versus δ 154s/128d observed for **4**. These shift trends provide unambiguous support for the assignment of C5-OCH₃ substitution. Finally, the ¹³C NMR shifts at all positions of **2** versus **4**, except at C5, C6, and C13a, differed by less than 2 ppm. This provided additional support for the correctness of structure **5** and the assignment of its NMR signals shown in Table 2.

(14) De Guzman, F. S.; Carte, B.; Troupe, N.; Faulkner, D. J.; Harper, M. K.; Concepción, G. P.; Mangalindan, G. C.; Matsumoto, S. S.; Barrows, L. R.; Ireland, C. M. *J. Org. Chem.* **1999**, *64*, 1400–1402.

(15) (a) Schmitz, F. J.; Bloor, S. J. *J. Org. Chem.* **1988**, *53*, 3922–3925. (b) Roll, D. M.; Scheuer, P. J. *J. Am. Chem. Soc.* **1983**, *105*, 6177–6178. (c) Nakamura, H.; Kobayashi, J.; Kobayashi, M.; Ohizumi, Y.; Hirata, Y. *Chem. Lett.* **1985**, 713–716. (d) Harada, N.; Sugioka, T.; Uda, H.; Kuriki, T.; Kobayashi, M.; Kitagawa, I. *J. Org. Chem.* **1994**, *59*, 6606–6613.

(16) (a) Harada, N.; Uda, H.; Kobayashi, M.; Shimizu, N.; Kitagawa, I. *J. Am. Chem. Soc.* **1989**, *111*, 5668–5674. (b) Kobayashi, M.; Shimizu, N.; Kitagawa, I.; Kyogoku, Y.; Harada, N.; Uda, H. *Tetrahedron Lett.* **1985**, *26*, 3833–3836. (c) Kobayashi, J.; Hirase, T.; Shigemori, H.; Ishibashi, M.; Bae, M. A.; Tsuji, T.; Sasaki, T. *J. Nat. Prod.* **1992**, *55*, 994–998.

(17) (a) Concepción, G. P.; Foderaro, T. A.; Eldredge, G. S.; Lobkovsky, E.; Clardy, J.; Barrows, L. R.; Ireland, C. M. *J. Med. Chem.* **1995**, *38*, 4503–4507. (b) Alvi, K. A.; Rodriguez, J.; Diaz, M. C.; Moretti, R.; Wilhelm, R. S.; Lee, R. H.; Slate, D. L.; Crews, P. *J. Org. Chem.* **1993**, *58*, 4871–4880. (c) Harada, N.; Sugioka, T.; Uda, H.; Kuriki, T. *J. Org. Chem.* **1990**, *55*, 3158–3163.

(18) ACD/CNMR v. 2.51; Advanced Chemistry Development Inc: Toronto, Canada, 1997.

TABLE 2. NMR Data^a for Neoamphimedine (**2**) in DMSO-*d*₆, 5-Methoxyneoamphimedine (**4**) in DMSO-*d*₆, Neoamphimedine Y (**5**) in CDCl₃:CD₃OD 2:1, and Neoamphimedine Z (**6**) in DMSO-*d*₆

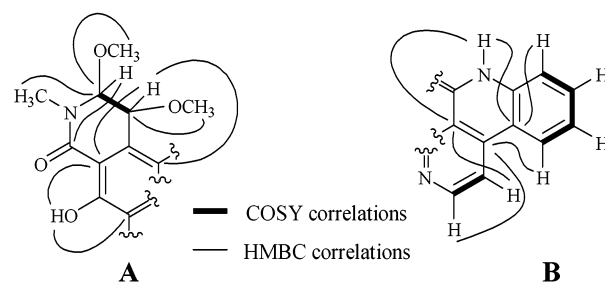
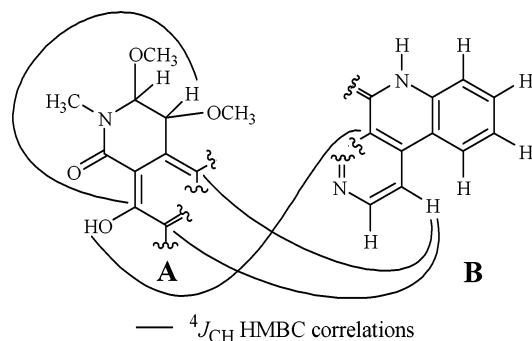
position	2		4		5		6		HMBC		
	δ_C	δ_H (J in Hz)	δ_C	δ_H (J in Hz)	δ_C^c	δ_H (J in Hz)	δ_C	δ_H (J in Hz)	$^3J_{CH}$	$^2J_{CH}$	$^4J_{CH}$
9	158.5		158.5		166.4		168.1				
6	148.2	9.27 d (5.5)	128.4	9.07 s	141.1	8.24 bs	151.3	8.61 d (4.8)	C4b	C5	C12c, C4a
8	178.5		177.9		149.4		149.7				
7a	147.5		146.9		143.2*		140.8				
13a	144.7		139.8		141.0		140.2				
4b	136.8		134.1		128.6*		139.4				
2	131.1	8.05 t (7.0)	131.1	8.04 t (7.77)	135.6	7.65 bdd (6.3, 8.0)	132.0	7.36 dd (8.0, 15.0)	C13a, C4		
12b	147.2		145.5		128.4*		128.8				
4	124.2	8.99 d (8.0)	124.4	9.42 d (7.77)	124.7	7.97 bd (6.3)	124.0	7.99 d (8.0)	C13a, C4b		C1
12c	117.5		118.5		121.6*		121.5				
3	130.1	7.98 t (7.0)	130.2	7.95 t (7.77)	123.1	7.22 bt (6.3)	120.6	6.96 t (8.0)	C1		C13a
1	132.0	8.36 d (7.0)	131.3	8.37 d (7.77)	117.6	7.78 d (8.0)	116.0	7.33 d (8.0)	C3, C4a		C4b
4a	122.3		121.7		113.7		115.0				
5	119.5	8.99 d (5.5)	154.4		107.4	7.53 bs	110.3	7.66 d (4.8)	C12c, C4a	C6, C4b	C7a, C12b
8a	119.2		119.0		112.8		107.4				
12a	150.2		149.3		110.3		104.4				
11	146.1	8.36 d (6.9)	144.8	8.33 d (7.17)	90.1	4.96 bd (2.0)	89.6	5.09 d (2.7)	C9, C12a, C14, NMe	C12	C15, NMe
12	99.6	7.65 d (6.9)	99.7	7.69 d (7.17)	67.7	5.50 bd (2.0)	67.6	5.26 d (2.7)	C12b, C8a, C15	C12a, C11	C8, C14
15			58.0	4.40 s			56.3	3.43 s	C11		
16							54.9	3.31 s	C12		
14	37.8	3.60 s	38.0	3.60 s	35.0	3.35 s	35.2	3.23 s	C11		C8a
OH							12.89 s		C7a, C8a	C8	C12c
NH							9.66 s		C12c, ^b C4a ^b		

^a Measured at 500 MHz (¹H) and 125 MHz (¹³C). ^bWeak correlation. ^cAn asterisk (*) indicates signals may be interchanged.

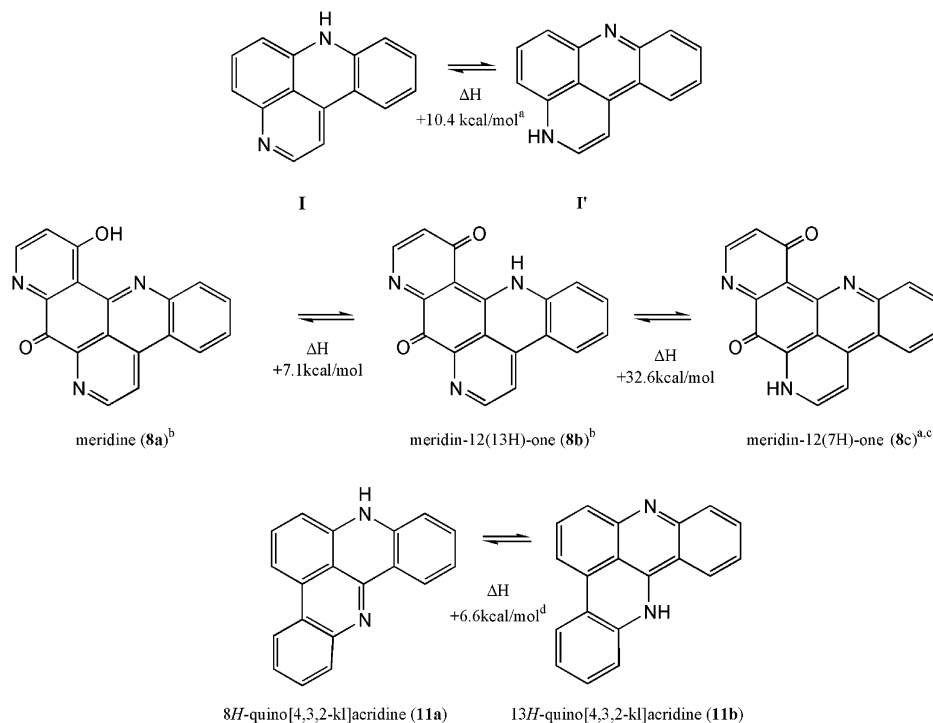
Neoamphimedine Y (**5**) and Z (**6**) were isolated as purple solids that turned brown upon standing. Preliminary ¹H and ¹³C NMR data for the purple samples revealed several signals for this pair that were similar to those observed for **2**. In addition, these data indicated that **5** and **6** differed by the two hydroxy groups of the former being replaced by two methoxy groups. Further analysis was not possible because of sample decomposition after 2 days at room temperature. Fortunately, neoamphimedine Z (**6**) could be re-isolated and was used for structure elucidation while also serving as the basis for the characterization of **5**. An additional complication was that neither compound reliably ionized during MS analysis ranging from ESI, FAB, to EI.

Even though the molecular formula for **6** could not be established from the MS data, it could be deduced from the NMR spectra. In addition these results provided insights to establish two major substructures. The ¹³C NMR spectrum (Table 2) revealed 15 vinyl carbons, one carbonyl (δ 168.1), two OCH₃ groups, one NCH₃ moiety, and two oxygen-substituted aliphatic carbons. A ¹H NMR spectrum in DMSO-*d*₆ showed two exchangeable protons at δ 12.89 (OH) and δ 9.66 (NH), plus three separate coupled spin systems: two aromatic sets and one aliphatic cluster. Collectively these data indicated a partial formula of C₂₁H₁₉O₄N₂ for **6**, somewhat analogous to that for **2** (C₁₉H₁₁O₂N₃). The gradient ¹H-¹H COSY NMR data summarized in Figure 1 plus analogies to the features of **2** provided insights to propose substructures **A** and **B**. These moieties also supplied a missing N to give a final formula for **6** of C₂₁H₁₉O₄N₃.

The structural features of **6** identified at this point included each of the four rings of structure **I**. These were justified by observing: the A-ring proton and carbon signals, the B (or D)-ring NH, the upfield carbon signals of the C-ring (8a, 12a), and the isolated AB spin system of the D-ring (H5, H6). A dihydro pyridone E-ring was identified from the two mutually coupled (J = 2.7 Hz)

**FIGURE 1.** ¹H-¹H COSY and selected HMBC correlations of neoamphimedine Z (**6**).**FIGURE 2.** Selected long-range HMBC correlations of neoamphimedine Z (**6**).

aliphatic protons (H11 and H12). A regular gradient HMBC experiment (Figure 1) featuring two and three bond couplings provided additional support for substructures **A** and **B**; however, these data did not provide insights about their interconnection. Biosynthetic considerations suggested the most logical way to join **A** and **B** would be to create the D-ring system present in **I**. In part, proof for this assumption was obtained by a second HMBC experiment with parameters set to emphasize ⁴J_{CH} correlations. Shown in Figure 2 are the

SCHEME 1. Semiempirical Molecular Orbital Calculated Tautomer Equilibrium Values among Annulated Acridines


^a Calculations from this work (see Supporting Information). ^bStructure reported in ref 20. ^cStructure not discussed in ref 20. ^dStructures and data from ref 19.

HMBC correlations between H5–C7a, H5–C12b, and OH–C12c that supported the final overall structure proposed as **6** and by extrapolation that proposed as **5**.

The final issue to be addressed in the characterizations of **5** and **6** involved dissecting out the relative contribution from tautomers **I/I'**. Pyridoacridines with an NH group are sometimes drawn in the literature as tautomer **I** but without supporting data to rule out **I'**. Structures shown in Scheme 1 illustrate situations where more than one tautomer could be expected. A revealing circumstance is provided by the co-isolation of meridine (**8a**) and meridin-12(13H)-one (**8b**) by Schmitz from a tunicate.²⁰ The former was the most stable isomer and it was characterized by X-ray analysis while the position of the NH group in the latter was established from NOE data. Likewise, X-ray measurements, NOE results, and semiempirical molecular orbital calculations proved that quinoacridine, obtained by synthesis, exists as structure **11a** rather than **11b** ($\Delta H = 6.6$ kcal/mol).¹⁹ Our gas-phase calculations (Scheme 1 and Supporting Information) are in agreement with these trends and show **I** is 7.1–9.7 kcal/mol lower in energy than **I'** and that the stability order for meridine is predicted to be **8a** > **8b** > **8c**.

We were unable to obtain NOE data for **5** or **6**; however, the ΔH data in Scheme 1 provide support for imbedding tautomer **I** in their structures. The same conclusion is supported by analysis of ¹H NMR shifts of the pyridoacridine A-ring protons and these data are collected in Table 3. The diagnostic pattern can be

assessed from analysis of shifts at H1,2,4,5 (in DMSO, CDCl₃, or CDCl₃:MeOH solvent mixtures). Those of amphimidine (**1**), neoamphimedine (**2**), 5-methoxyneoamphimidine (**4**), and meridine (**8a**) are diagnostic for the A,B-ring type present in **I'**, whereas those of meridin-12(13H)-one (**8b**),²⁰ *N*-deacetylguanoniamine C (**9**),^{12e} styelsamine C (**10**),^{12d} and 13H-quinoacridine (**11a**) provide shifts expected for the A,B-ring type in **I**. Thus, when tautomer **I'** dominates, proton chemical shifts will be greater than δ 7.8 at H1 and H2, and greater than δ 8.6 at H4 and H5. Alternatively, the diagnostic values for **I** consist of shifts that are less than δ 7.8 for H1, H2, and H5, and less than δ 8.6 for H4. Thus, the proton shifts of **6** (H1/2/4/5 at δ 7.33/7.36/7.99/7.66) and **5** (H1/2/4/5 at δ 7.78/7.65/7.97/7.53) both match the pattern for form **I**.

The relative stereochemistry assigned for the E-ring vicinal oxygens of **5** and **6** was based on interpreting the ³*J*_{11,12} = 2.0 and 2.7 Hz, respectively. The singular model compound in the literature was lysolipin I (**12**),²¹ with a ³*J*_{23,24} = 4.2 Hz. Further data were derived from molecular modeling using the two diastereomers of hypothetical compound **13**,²² giving calculated ³*J*_{cis} = 3.01 Hz and ³*J*_{trans} = 7.75 Hz. This close agreement between the experimental and calculated *cis* *J* values and the large difference between calculated *cis* vs *trans* couplings provided the final information in support of the *cis* stereochemistry shown for both **5** and **6**.

The final compound to be analyzed, alpinkidine (**7**), was obtained as a purple solid after successive HPLC runs.

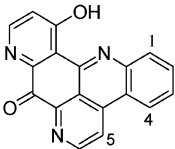
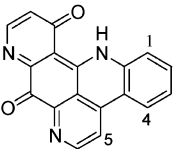
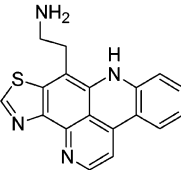
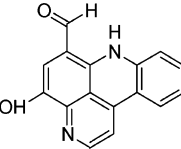
(19) Hagan, D. J.; Giménez-Arnau, E.; Schwalbe, C. H.; Stevens, M. F. G. *J. Chem. Soc., Perkin Trans. S* **1997**, 2739–2746.

(20) Schmitz, F. J.; DeGuzman, F. S.; Hossain, M. B.; van der Helm, D. *J. Org. Chem.* **1991**, 56, 804–808.

(21) (a) Bockholt, H.; Udvarnoki, G.; Rohr, J.; Mocek, U.; Beale, J. M.; Floss, H. G. *J. Org. Chem.* **1994**, 59, 2064–2069. (b) Dobler, M.; Keller-Schierlein, W. *Helv. Chim. Acta* **1977**, 60, 178–185.

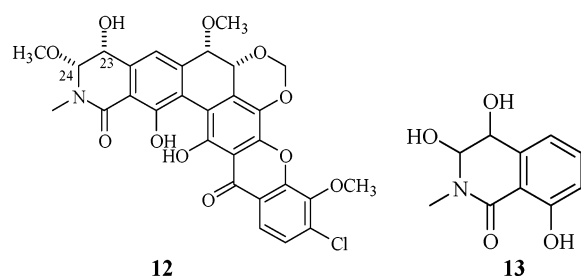
(22) PC-Model v 7.0; Serena Software, 1999.

TABLE 3. ^1H NMR Data^a (δ_{H}) for **2**, **5**, **6**, **8a**, **8b**, **9**, and **10**

								
	8a	8b	9	10				
position	2 ^b	2 ^c	8a ^{20,c}	5 ^d	6 ^b	8b ^{20,c}	9 ^{12e,b}	10 ^{12d,b}
1	8.36	7.98	8.23	7.78	7.33	7.44	7.40	7.61
2	8.05	7.82	7.97	7.65	7.36	7.63	7.40	7.61
3	7.98	7.73	7.86	7.22	6.96	7.38	7.02	7.28
4	8.99	8.84	8.64	7.97	7.99	8.20	8.06	8.33
5	8.99	8.85	8.66	7.53	7.66	7.64	7.68	7.93
6	9.27	9.21	9.38	8.24	8.61	8.94	8.67	8.80

^a Measured at 500 MHz (^1H). ^b DMSO-*d*₆. ^c CDCl₃. ^d CDCl₃:MeOH-*d*₄ 2:1.

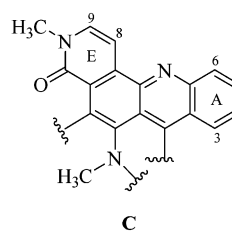
CHART 4

TABLE 4. ^1H NMR Data of Plakinidine A (**3**) in DMSO-*d*₆, Alpkindine (**7**)^a in CDCl₃, and Neoamphimedine (**2**)^a in DMSO-*d*₆

3	7	2				
<hr/>						
position	3 ²	7	position	2		
	δ_{H}	$^3J_{\text{H-H}}^b$	δ_{H}	$^3J_{\text{H-H}}^b$	δ_{H}	$^3J_{\text{H-H}}^b$
2	8.47 s				1	8.36 d 7.0
3	8.42 d 7.8	8.98 d 8.4	2	8.05 t 7.0		
4	7.73 t 7.2	7.87 m	3	7.89 t 7.0		
5	7.69 t 9.3	7.87 m	4	8.99 d 7.0		
6	8.27 d 8.1	8.48 d 7.95	5	8.99 d 5.5		
8	9.93 brs	7.53 d 7.2	6	9.27 d 5.5		
9	3.82 dt 7.8 1.2	8.10 d 7.2	11	8.36 d 6.9		
13	11.17 q 5.4	3.84 s	12	7.65 d 6.9		
14	3.68 d 5.7	3.80 s	14	3.60 s		
10	2.72 t 7.8					

^a Measured at 500 MHz (^1H). ^b In hertz.

It was not possible to gather MS data by ESI, FAB, or EI, which is similar to the situation noted above for some of the other acridine derivatives. The ^1H NMR data for **7** shown in Table 4 revealed only six aromatic protons and two NCH_3 groups. The ^1H – ^1H COSY spectrum confirmed an isolated AB pattern for two protons, eventually assigned as H8–H9, along with a separate four-spin system, eventually assigned as H3–H4–H5–H6. A minor complication was that the resonances of H4 and

FIGURE 3. Substructure of alpkindine (**7**).

H5 were isochronous. Attempts to obtain acceptable ^{13}C NMR data on **7** failed due to its low solubility, limited sample size (2.0 mg), and the long relaxation times of the quaternary carbons. Consequently, there was little available information to continue with the structure elucidation. However, the rich purple color, a biosynthetic analogy to the other compounds encountered so far, and the very downfield shifts of the four-spin ^1H system suggested the presence of an acridine core. Further, an acridine A-ring could be inferred as all such known marine products have this ring annulated at C4a/C13a and not at C2/C3 (see **2** for numbering). Drawing on the correlation discussed above for the shifts of H1, H2, and H4 (see Table 3) it appeared that **7** also had fully conjugated A/B rings. The relatively downfield shift and diagnostic coupling constant magnitude of H9 (δ 8.10, J = 7.2 Hz) indicated this proton was α to an aromatic nitrogen and vicinal to H8 (δ 7.53, J = 7.2 Hz). Also, a comparison of these ^1H NMR data to that of neoamphimedine (**2**) revealed these shifts were more consistent with the protons of a E-ring (**2** δ 7.56/8.36) rather than of a D-ring (**2** δ 8.99/9.27). In addition, the coupling of these E-ring protons in **7** and **2** was larger than that seen for most pyridine rings but consistent with that observed for a pyridone ring system.

Alpkindine (**7**) appeared to have features in common with those of A,B,C,E-rings of **2** and **4** isolated from this same sponge, but there were not enough data in hand at this point to further define the structure. The best that could be done was to envision a partial structure **C** (in part based on methylation of a type-I' tautomer) shown in Figure 3. It was fully consistent with the accumulated information and was compatible with a biosynthetic analogy that could be drawn to other pyridoacridines. The limited available NMR data made it impossible to gener-

ate the other undefined substructures that must be present. Fortunately, several small crystals were obtained by slow evaporation of a solution of alpinkidine in CDCl_3 . The X-ray analysis was then conducted leading to the final structure of **7** (see perspective drawing of Scheme S1). As expected from this result, close analogies exist among the structures and ^1H NMR properties summarized in Table 4 for alpinkidine (**7**), amphimedine (**2**), and plakinidine A (**3**).

Conclusions

The most significant new chemotype isolated in this study was the pyrroloacridine, alpinkidine (**7**). It has an unprecedented overall nitrogen heterocyclic framework with uniquely positioned oxygen functionality. Since **7** shares the pyrroloacridine framework with that of **3** and the other plakinidines also reported from both a sponge (*Plakortis* sp.^{2,9c}) and a tunicate (*Didemnum rubeum*^{9a}) it was therefore numbered in a similar manner and named alpinkidine to reflect the switch of C8 and N10 between this pair!

Another striking feature of our results was the isolation of pyridoacridine **2** as the major metabolite along with the absence of meroterpenoids from two different species of sponges in the genus *Xestospongia* collected in widely different Indo-Pacific locales (Papua New Guinea and Indonesia). Added to this circumstance is that pyridoacridines have been isolated from ascidians, sponges, and one prosobranch,¹ although the latter example is likely due to accumulation of the alkaloids from dietary intake. The compounds reported above can be added to the list of pentacyclic acridines, all of marine origin, that are divisible into five structural classes based on their individual carbon–nitrogen skeletons (see Table S2, Supporting Information). Also noteworthy is that tetracyclic acridines have not been isolated from sponges, as such compounds seem to be restricted to tunicates. It is uncommon to find instances of related or identical compounds isolated from more than one phylum. In this regard, the pyridoacridine neoamphimedine Y (**5**) is somewhat related to meridine (**11a**) previously reported from both a sponge (*Corticum* sp.²³) and a tunicate (*Amphicarpa meridiana*²⁰). Thus, both pyridoacridines and pyrroloacridines are clearly products of a biosynthetic pathway common to marine invertebrates in different phyla, but the factors responsible for this unusual circumstance have so far eluded definition. Finally, the isolation of a pyrroloacridine in conjunction with a pyridoacridine is unparalleled.

The similarities in the overall skeletons of neoamphimedine (**2**) and alpinkidine (**7**) suggest the possibility of a common biosynthetic starting point in their biosynthesis. The outline and discussion of Scheme S2 provides some details supporting this supposition and illustrates that tryptophan can be a universal building block. It draws on the biosynthesis of shermilamine B (**14**) that was rigorously examined by Steffan²⁴ using feeding experiments with a tunicate-derived cell-free extract

showing both *S*-[5- ^3H]tryptophan and [7,8- $^3\text{H}_2$]dopamine are incorporated in the formation of **14**.

The major biological properties discovered for pyridoacridines involve DNA intercalation and binding to receptors such as DNA topoisomerases.¹ One interesting recent finding is that amphimedine (**1**) and neoamphimedine (**2**) dramatically differ in their ability to facilitate catenation of DNA by topoisomerase II,¹⁴ with the latter being active and the former not. Also relevant is that 9-deoxyamphimedine⁶ is more potent than **1** or **3** in DNA cleavage assays. Samples of **1**, obtained from our compound repository, and **7** were found to be solid tumor selective in the disk diffusion soft agar colony assay only against murine cell lines (see Table 1, entries 14 and 17), with **7** about 30-fold less potent than **1**. On the other hand, neoamphimedine (**2**) was both murine and human solid tumor selective, while 5-methoxyneoamphimedine (**4**) proved to be the most murine solid tumor selective compound in the assay. It appears that the cross-conjugated enone arrangement present in the C,E-rings of **2** accentuates the biological activity that is further amplified by D-ring OCH_3 functionalization. Interestingly, during the course of bioassay guided purification the data collected revealed the compounds were more solid tumor selective than the extract fractions. This circumstance further indicates the effectiveness of the disk diffusion soft agar assay as an initial discovery tool. Overall, the tumor selectivity results obtained suggest that **2** and its analogues deserve further preclinical evaluation. Such studies are underway with **2** in tumor-bearing mice to better define its pharmacological properties and these results will be reported elsewhere.

Experimental Section

General Experimental Procedures. The NMR spectra (CDCl_3 :MeOH- d_4 2:1 and DMSO- d_6) were recorded at 500 MHz (^1H) and 125.7 MHz (^{13}C). Final NMR assignments were based either on previously published data¹⁴ or 2D NMR data derived from gHMBC, gHMBC, and ^1H – ^1H gCOSY. The normal gradient HMBC experiment (Figure 1) used a coupling of 8 Hz (65 ms dephasing) for 3-bond correlations and the special experiment (Figure 2) long-range coupling of 4 Hz (127 ms dephasing) for 4-bond correlations. Diaion HP-20 (Mitsubishi Kasei) polymeric resin was used for separation of the crude fraction. HPLC was performed with a reverse-phase Phenomenex 5- μm LUNA column.

Biological Material, Collection, and Identification. Specimens of *Xestospongia* cf. *carbonaria* (coll. no. 94634) and *Xestospongia* cf. *exigua* (coll. no. 91608) were collected from Indonesia and Papua New Guinea, respectively, using SCUBA, at depths of 20–100 feet. The two sponges are similar but clearly belong to different species.

Xestospongia cf. *carbonaria*²⁵ is a massive-ramose, branching sponge, black to dark green externally, and black internally. The surface was smooth and the sponge was hard in consistency. Simple round oscules (5 mm in diameter) were dispersed on the topside of branches. The skeleton in the choanosome possessed a multispicular reticulation with primary tracts running toward the surface and thinner secondary tracts connecting them. Many spicules were singly strewn between the major spicule tracts, and the ectosome was formed by single spicules loosely strewn tangentially. The spicules are slender thin fusiform oxeas, 250–270 \times 6–8 μm .

Xestospongia cf. *exigua*²⁶ is a ramose, green-black sponge, with smooth branches 1 cm in diameter, and >10 cm high. It has a smooth surface that is hard in consistency but is also porous with round oscules (3–4 mm in diameter) dispersed

(23) McCarthy, P. J.; Pitts, T. P.; Gunawardana, G. P.; Kelly-Borges, M.; Pomponi, S. A. *J. Nat. Prod.* **1992**, *55*, 1664–1668.

(24) Steffan, B.; Brix, K.; Puetz, W. *Tetrahedron* **1993**, *49*, 6223–6228.

regularly in one side of the branches. The skeleton in the choanosome possesses a spicular reticulation of thick multispicular tracts (100–150 μm in diameter). In the ectosome the multispicular tracts are thinner (30–50 μm in diameter), and are filled in with an isotropic unispicular reticulation. The spicules are oxeas that ranged in size from 220 to 290 \times 4–20 μm , and have shapes ranging from thin fusiform oxeas to stout stronglyloxeas. The large spicule size and spicule size range is rather atypical of *X. exigua*, usually reported with smaller spicule sizes. Therefore the specimen is considered close to *X. exigua* but with differences that may indicate a different species identity.

Extraction and Isolation. The sponges were initially preserved according to our standard procedure as described previously⁸ and then transported to the home laboratory at ambient temperature. Each collection was worked up separately. The solvent (100% methanol) was added and the organisms were soaked three successive times for 24 h. The solvent was evaporated at room temperature and the resulting oil partitioned between water (the *sec*-butyl alcohol soluble sample coded “WB”) and CH_2Cl_2 (sample coded “F”). The concentrated F was next partitioned between hexanes (sample coded “FH”) and 10% aqueous MeOH to remove unwanted lipids and steroid components. The MeOH layer was adjusted to 50% aqueous MeOH and an equal volume of CH_2Cl_2 was added. The CH_2Cl_2 fraction (coded “FD”) and the MeOH fraction (coded “FM”) were evaluated separately. The sponges were soaked additionally two times in CH_2Cl_2 and the resulting crude oil was repeatedly partitioned between equal volumes of 10% aqueous MeOH and hexanes. The hexanes fraction was coded as “DMH” and the MeOH fraction was coded “DMM”.

Pure compounds were obtained as follows. The “FD” sample of *Xestospongia* cf. *exigua* (21 mg) was prioritized for HPLC because of the activity shown in Table 1. The separation scheme (Chart 1) employed a solvent gradient from 1:1 up to 0:100 H_2O :MeOH (0.1% formic acid in both solvents) to yield **2** (6.8 mg) and **4** (0.7 mg). The “DMM” sample of *Xestospongia* cf. *carbonaria* was chosen for follow-up due to the positive activity shown in Table 1. It was subjected to chromatography on Diaion HP-20 and eluted with H_2O :MeOH 9:1 (sample coded “HP1”), H_2O :MeOH 1:1 (sample coded “HP2”), 100% MeOH (sample coded “HP3”), and 100% acetone (sample coded “HP4”). The last three fractions were further purified using gradient reverse-phase HPLC (H_2O :MeOH 1:1 up to 0:100 with 0.1% formic acid in both solvents) to yield **2** (21.8 mg), **4** (3.4 mg) **5** (2.2 mg), **6** (4.0 mg), and **7** (2.0 mg) as shown in Chart 2.

Disk Diffusion Soft Agar Colony Formation Assay. An *in vitro* cell-based assay was employed to identify solid tumor selectivity for original extracts, extract partition fractions, and pure compounds. The differential cytotoxicity²⁷ is expressed by observing a zone differential between any solid tumor cell (Colon38, ColonH116, Lung H125) and either leukemia cells (L1210 or CEM) or normal cells (CFU-GM). A sample is designated as “solid tumor selective” if (zone units of solid tumor – normal cells or leukemia cells) is greater than 250 units. The activity results appear in Tables 1 and S1.

Neoamphimedine (2): yellow solid; HRESIMS obsd m/z 314.0945 (calcd for $\text{C}_{19}\text{H}_{12}\text{N}_3\text{O}_2$ [$\text{M} + \text{H}$]⁺ 314.0930, Δ 1.5 mmu). ^1H NMR (500 MHz) and ^{13}C NMR (125 MHz) in Table 2.

(25) van Soest, R. W. M. *Marine sponges from Curaçao and other Caribbean localities, Part II: Haplosclerida*; Stud Fauna Curaçao Caribb. Isl., 1980.

(26) Bergquist, P. R. *The sponges of Micronesia, Part I: The Palau archipelago*; Pac Sci 1965.

(27) Valeriote, F.; Grieshaber, C. K.; Media, J.; Pietraszkiewicz, H.; Hoffman, J.; Pan, M.; McLaughlin, S. J. *Exp. Ther. Oncol.* **2002**, *2*, 228–236.

5-Methoxyneoamphimedine (4): yellow solid; HRESIMS obsd m/z 344.1044 (calcd for $\text{C}_{20}\text{H}_{14}\text{N}_3\text{O}_3$ [$\text{M} + \text{H}$]⁺ 344.1035, Δ 0.9 mmu); ^1H NMR (500 MHz) in Figure S1 and Table 2; ^{13}C NMR (125 MHz) in Figure S2 and Table 2; ACD calculated spectrum of 5-methoxyneoamphimedine in Figure S13; and ACD calculated spectrum of 6-methoxyneoamphimedine in Figure S14.

Neoamphimedine Y (5): purple solid, which turns brown upon standing; ^1H NMR (500 MHz) in Figure S3 and Table 2; ^{13}C NMR (125 MHz) in Figure S4 and Table 2.

Neoamphimedine Z (6): purple solid, which turns brown upon standing; ^1H NMR (500 MHz) in Figure S5 and Table 2; ^{13}C NMR (125 MHz) in Figure S6 and Table 2. Additional NMR data include ^1H – ^1H gCOSY in Figure S7, gHMQC in Figure S8, gHMBC in Figure S9, and long-range gHMBC in Figure S10.

Alpinkidine (7): purple solid, which turns green upon addition of acid; ^1H NMR (500 MHz) in Figure S11 and Table 4; ^1H – ^1H gCOSY in Figure S12; but ^{13}C NMR data could not be obtained. The single-crystal X-ray analysis was conducted as follows. A dark, needle-shaped crystal (0.80 \times 0.10 \times 0.05 mm³) was mounted on a Bruker SMART diffractometer (Mo K α ; –100 °C). A hemisphere of data was taken using a narrow-scan routine (1406 frames, 0.3° step ω -scan, exposure time of 30 s/frame, $2\theta_{\text{max}}$ = 49.42°). Raw data were integrated with the Bruker SAINT+ program to yield a total of 10377 reflections, of which 2454 were independent (R_{int} = 6.44%, completeness 99.9%) and 1793 with $I > 2\sigma(I)$. Data were corrected for absorption using the SADABS program (min. and max. transmission are 0.5547 and 0.9947, respectively). The structure was solved by direct methods²⁸ and refined by full matrix least squares on F^2 techniques²⁸ using anisotropic displacement parameters for all non-hydrogen atoms. All hydrogen atoms were found in the difference Fourier map and refined isotropically. At final convergence, R_1 = 4.91% and GOF = 0.930 for 278 parameters. Additional information about these data includes crystal data and structure refinement in Table S3, atomic coordinates in Table S4, bond lengths and angles in Table S5; anisotropic displacement parameters in Table S6; and hydrogen coordinates in Table S7.

Acknowledgment. Financial support at UCSC and JFCC was from NIH grant CA47135. Sponge taxonomy analyses were generously provided by Dr. M. Cristina Diaz (UCSC). Additional financial support at UCSC was from equipment grants from NSF BIR-94-19409 (NMR) and the Elsa U. Pardee Foundation (ESI-Quadrupole MS) and a supplement to NIH CA52955 for the purchase of the ESI-TOF-MS. The Cornell group was partially supported by NIH grant CA24487. Special thanks to Prof. J. Supratana of the University of Jakarta for his invitation to conduct scientific research and to the crew of the *M/V Serenade* for their assistance during the expedition in Indonesia. We are also grateful to Dr. D. Niles of the Institute of Papua New Guinea Studies for assistance with research permit formalities and to Mr. Vanderloos, Skipper of the PNG vessel *M/V Chertan*, for his enthusiastic assistance.

Supporting Information Available: NMR spectra of **4** (^{13}C and ^1H), **5** (^{13}C and ^1H), **6** (^{13}C , ^1H , ^1H – ^1H , HMQC, HMBC, and long-range HMBC), and **7** (^1H) as well as X-ray data and NMR simulation data. This material is available free of charge via the Internet at <http://pubs.acs.org>.

JO0264590

(28) Sheldrick, G. M. *Shelx 86*, a computer program for crystal determination; University of Göttingen: Göttingen, 1986.